NASA Technical Memorandum 87335

Centaur Engine Gimbal Friction Characteristics Under Simulated Thrust Load

James W. Askew
Lewis Research Center
Cleveland, Ohio

September 1986

NASA

Trade names or manufacturers' names are used in this report for identification only. This usage does not constitute an official endorsement, either expressed or implied, by the National Aeronautics and Space Administration.

CENTAUR ENGINE GIMBAL FRICTION CHARACTERISTICS UNDER SIMULATED THRUST LOAD

James W. Askew
National Aeronautics and Space Administration
Lewis Research Center
Cleveland, Ohio 44135

ABSTRACT

An investigation was performed at NASA Lewis Research Center to determine the friction characteristics of the engine gimbal system of the Centaur upper stage rocket. Because the Centaur requires low-gain autopilots in order to meet all stability requirements for some configurations, control performance (response to transients and limit-cycle amplitudes) depends highly on these friction characteristics. Forces required to rotate the Centaur engine gimbal system were measured under a simulated thrust load of 66 723 N (15 000 lb) and in an altitude/thermal environment. A series of tests was performed at three test conditions: ambient temperature and pressure, ambient temperature and vacuum, and cryogenic temperature and vacuum. Gimbal rotation was controlled, and tests were performed in which rotation amplitude and frequency were varied by using triangular and sinusoidal waveforms. Test data revealed an elastic characteristic of the gimbal, independent of the input signal, which was evident prior to true gimbal sliding. The torque required to initiate gimbal sliding was found to decrease when both pressure and temperature decreased. Results from the low amplitude and low frequency data are currently being used in mathematically modeling the gimbal friction characteristics for Centaur autopilot performance studies.

E-3080

NOMENCLATURE

CF coulomb friction

K slope of spring constant of gimbal

K_1 slope of spring constant of test rig

T friction torque

δ rotation angle

$\dot{\delta}$ angular velocity

INTRODUCTION

Thrust vectoring, one method used for space vehicle flight control, is typically accomplished by a servocontrolled actuator system, which rotates a rocket engine nozzle about a single gimbal point. Such a system is incorporated in the Centaur upper stage vehicle. The dynamics of rotating the engine about the gimbal point depends highly on the friction characteristics of the gimbal. For Centaur, a hydraulic power unit is used to actuate engine motion about a two-axis gimbal system that mounts the engine to the vehicle. The gimbal system also provides the load path into the vehicle structure for engine thrust.

Background

The design of the Centaur D1-A powered phase autopilot and the resulting assessment of control performance depended on reliable, test-verified mathematical models. These mathematical models, over the history of the Centaur D1 and Centaur D1-A, have been shown to be accurate representation of the hardware and software flown. This has been demonstrated through component level testing and flight performance evaluation. The current design of the autopilot was first flown on April 5, 1973. Payloads have ranged in weight from approximately 500 to 3085 kg (1100 to 6800 lb). The autopilot configuration has remained constant with variations only in constants required for optimization. This design is also being applied to the shuttle/Centaur for those payloads which have dynamic and weight characteristics similar to payloads previously flown on D1-A. Classes of payload which are different than those previously flown may require a redesign of the autopilot control

law. In particular, for payloads which require low-gain autopilots, performance depends highly on the friction characteristics of the engine gimbal. This high dependence on engine gimbal friction resulted in a test program to further refine a friction mathematical model.

In the time period between 1962 and 1965, two tests were run to determine the friction characteristics of the engine gimbal. A hot firing test was run at NASA Lewis Research Center, and a static load test was run at Pratt & Whitney, the engine manufacturer. Both of these tests showed values of coulomb friction from 71 to 91 J (52 to 67 ft-lb) per plane. These results were well below the specified requirement of 271 J (200 ft-lb) set by General Dynamics Space System Division for a 66 723-N (15 000-lb) thrust engine.

Purpose

A more accurate measurement of the friction characteristics of the present Centaur gimbal system was needed to properly assess autopilot performance for certain shuttle/Centaur applications. The purpose of this test was to determine the friction characteristics of the Centaur engine (model RL10A-3-3A) gimbal system, under thrust load and in an altitude/thermal environment.

APPARATUS

Engine Mount Gimbal Assembly

The gimbal mount assemblies used for the tests were Pratt & Whitney RL10A-3-3A engine flight gimbals. The gimbal mount assembly provided a universal bearing system to allow gimbaling of the engine for thrust vectoring (Fig. 1). The gimbal assembly, as described in Ref. 1, consisted of a conical engine mount, a pedestal, and a spider block. Gimbaling was accomplished by rotation about the spider block, which connected the pedestal to the conical mount. The gimbal incorporated dry-lubricated journal bearings, which permitted gimbal movement of ±4° in a square pattern during engine operation. The gimbal assembly was secured to the test rig by four bolts, which passed

through the top of the pedestal. The gimbal assembly was instrumented with two thermocouples to monitor temperature on the pedestal and conical section during cryogenic testing.

Test Facility

The vacuum facility used in testing was the Super Bell Jar facility located at Lewis. This facility consists of two separate stainless steel bell jars; however, only one was used for the testing described. Each bell jar has a 86.36-cm (34.0-in.) diameter and is 170.18 cm (67.0 in.) high. A single 88.9-cm-diameter (35-in.-diam) oil diffusion pump was mounted on the bottom of the bell jar. Pressure in the bell jar during testing was maintained between 0.041 and 5.068 N/m^2 (5.88×10^{-6} and 7.35×10^{-4} psi). The gimbal mount assembly was mounted from a specially designed top flange plate (test rig, Fig. 2) with the conical section pointing downward along the bell jar axis.

A variable-displacement hydraulic pump was used during testing to provide the proper flow rate of 1.58×10^{-4} m^3/sec (2.5 gal/min) and pressure of 3.45×10^6 N/m^2 (500 psig) needed to supply the closed-loop servocontrolled actuator. The pump was in operation only when an oscillation signal was commanded to the closed-loop servocontroller, resulting in actuator movement.

Liquid nitrogen was used in the test rig as a coolant to simulate the cryogenic temperature of the liquid oxygen tank (94 K or 170 °R). The liquid nitrogen was transferred from a conventional pressurized (1.72×10^5 N/m^2 or 25 psig) Dewar to the test rig cold plate by foam-insulated lines. However, before the test rig was submitted to cryogenic temperature, a gaseous nitrogen purge on the bell jar was performed. This evacuated moisture from the environment to prevent ice from forming on the gimbal (test rig). Gaseous nitrogen was also used to pressurize the pneumatic load applicator (bellows), which was used to apply a compression load to the gimbal for simulating engine thrust.

Test Rig

The test rig used to determine the gimbal friction characteristics was designed to incorporate a simulated thrust load of 66 723 N (15 000 lb), a space environment, and cryogenic temperatures. The fixture was optimized around two minimum-friction knife edge load rods (see Fig. 3). Further consideration included a common axis of rotation for the load rods and the journal bearings, constant load application throughout gimbal position, and a closed-loop response system.

The rig was designed and assembled by Pratt & Whitney. The basic design consisted of a large steel plate which was placed on one end of the environmental vacuum chamber (see Fig. 2). Mounted on the plate was an aluminum plug with passages for flowing liquid nitrogen. Inside the vacuum chamber was the gimbal mount assembly, the calibrated knife edge load rods, and the pneumatic bellows plate for applying load. Through the steel base plate, which was sealed with a bellows, the actuator rod hydraulically actuated the gimbal. Gaseous nitrogen, used to apply load to the bellows plate, passed through a bulkhead fitting to the inside of the vacuum chamber. The other testing fluids, liquid nitrogen for cooling and hydraulic oil for actuation, were kept external to the chamber.

PROCEDURE

Gimbal Movements

Gimbal position was controlled by a servocontrolled actuator. The input signals for triangular and sinusoidal wave patterns were supplied by a wide-range-frequency function generator. These input command signals were sent to the servoamplifier, which operated the actuator piston and rod. A linear variable differential transformer (LVDT) position feedback transducer was mounted normal to the piston rod (see Fig. 3). The LVDT measured the displacement of the actuator piston, which is relative to the gimbal

displacement. The signals from the LVDT were then fed back to the servoamplifier. The signals from the servoamplifier were recorded on a digital data recorder capable of recording 500 samples/sec and on a direct-writing oscillograph.

The LVDT feedback transducer calibration, which determined the output of the feedback transducer in volts per degree of gimbal displacement, was made prior to testing. The procedures (gimbal movement patterns) used for the various tests are described in the section Test Conditions.

Force Measurements

At the beginning of each test sequence, the gimbal was loaded with a compression force of 66 723 N (15 000 lb), representing the thrust load on the gimbal in flight. This was accomplished by pressurizing the bellows placed between plates A and B, shown in Fig. 3. The force generated between the two plates placed the gimbal and the two tension rods mounted on knife edges in compression. The knife edges were aligned to coincide with the centerline of the axis of rotation. This minimized forces (torques) from the loading mechanism as the gimbal rotated.

Forces applied to the gimbal were determined by a universal flat compression-tension load cell, which measured the forces being applied to the actuator (Fig. 3). The load cell was mounted on a support coaxially with the actuator rod, below the actuator. The location of the load cell was essential to the applied forces in order to neglect inertial forces. Loads to the load cell were applied through the actuator rod, which was concentric with the threaded hole at the center of the cell. Loads measured away from the support mount were considered tension loads, with positive signals. Loads measured toward the support mount were considered compression loads, with negative signals. The load cell signals were also recorded on the digital data recorder and the oscillograph.

The load cell calibrations, which determined the output signal in volts per newton (pound of force), were also made prior to testing. The applied forces were converted to applied torques by multiplying the force by the distance from the actuator rod to the pivot point of the gimbal.

Test Conditions

Three different test conditions were used during testing: (1) ambient temperature and pressure, (2) ambient temperature and vacuum, and (3) cryogenic temperature and vacuum. Test conditions 1 and 2 consisted of four test sequences each. The sequences were performed at frequencies of 0.1, 0.5, 1.0, and 2.0 Hz at an amplitude of 0.25° relative to the null position. Each sequence had a triangular wave input signal. Test condition 3 consisted of 12 sequences, which comprised both triangular and sinusoidal wave input signals. At this test condition, test sequences were performed at frequencies of 0.1, 0.5, 1.0, and 2.0 Hz, with amplitudes of 0.25° and 2.0° relative to the null position. See Tables I and II for test results of each sequence.

After completion of test condition 1, the bell jar was pumped down to a vacuum environment of 0.041 N/m^2 (5.88×10^{-6} psi), or below. Prior to test condition 3, the cold plate was cooled to a temperature of 94 K (170 °R).

THEORETICAL INVESTIGATION

Solid Friction

Solid friction is a quasi-static phenomenon that occurs when two solid surfaces are subjected to contact bond stress by external or inertial forces.[2] Both coulomb friction (CF) and static friction (stiction) are involved. The coulomb friction is related to the interface bond rupture stress, whereas the static friction, or stiction, is related to the maximum, or ultimate, stress of the interface bond. Figure 4 depicts the general characteristics of solid friction. When the velocity is equal to zero, stiction occurs. Further, as

velocity is applied, the friction force (torque) drops to a lower level, coulomb friction. This friction remains constant as the velocity increases.

Solid friction encompasses two different types of friction: sliding friction and rolling friction. However, since the gimbal assembly incorporates a journal bearing, rolling friction will be our primary concern.

Rolling Friction

Early theories of rolling friction attributed it to interfacial slip between the rolling element and the surface. However, rolling friction is now attributed to the deformation losses in the solid itself, although some slip may occur. With elastic solids, where no permanent deformation occurs, rolling friction is attributed to hysteresis losses in the solid. In rolling friction, the interface cohesively bonded regions are compression stressed on the front side of the contact area and tension stressed on the back. The process of rolling friction starts from an unstressed region between two solid surfaces. Thus, as the strain or relative displacement of the surfaces increases, the surfaces are elastically stressed until a critical stress between the two surfaces is reached. This critical stress is the interface bond rupture stress (coulomb friction). After the interface bond has been ruptured, the rolling surface begins to slide, and the rolling friction becomes sliding friction. The coulomb friction value remains constant until the relative displacement is reversed. The same effect occurs in the reverse direction, forming an elastic hysteresis. This force-versus-motion characteristic is similar to that shown in Fig. 5. Additional information can be obtained from Refs. 3 to 5.

RESULTS AND DISCUSSION

A series of tests was performed on five flight gimbals; however, only data for gimbals designated 759 and 94 are presented in Tables I and II. Graphic representations of the experimental data are depicted in Figs. 6 to 8. Figure 6 shows the contrasting characteristics of the high and low amplitudes,

whereas Fig. 7 depicts the contrast in test conditions. The data graphed in Figs. 6 and 7 have frequencies of 2 and 1 Hz, respectively. Figure 8 compares the characteristics of the input signals, sinusoidal and triangular, at an amplitude of 0.25° and a frequency of 0.1 Hz. Both pitch and yaw axes of rotation, on each gimbal, were tested under the three conditions specified earlier. An initial test sequence was run at the beginning of testing on each gimbal to determine the break-in characteristic. The force (torque) levels required to move the gimbals decreased with increasing number of cycles, leveling off after about 10 cycles. This data is not presented here.

Before each series of tests, several calibrations of the test rig were performed with a dummy gimbal to determine the inherent frictional characteristic of the test rig. This device had dimensions similar to a flight gimbal assembly, except that a knife edge replaced the pedestal and spider block. The data from these calibrations are not presented here. However, the data showed the test rig to have a linear variation (K1) of increasing force (torque) with increasing relative gimbal displacement (see Fig. 5(a)). This variation K1 was subtracted from data taken during gimbal testing. This data reduction resulted in a gimbal friction characteristic similar to that shown in Fig. 5(b).

Early testing on the RL-10 engine gimbal mounts,[6] showed the gimbal friction characteristic as shown in Fig. 4, for solid friction. However, in this test, data showed the fiction characteristic to be as that of rolling friction (see Fig. 5(b)).

The low-amplitude triangular and sinusoidal wave oscillations gave values of coulomb friction in a range of 90 to 129 J (66 to 95 ft-lb) in the pitch axis of rotation, and a range of 61 to 207 J (45 to 153 ft-lb) in the yaw axis. A linear variation of increasing force (torque) with increasing gimbal rotation

occurred when motion was reversed. This slope (K) lasted over an interval of 0.2° and decreased with increasing frequency (see Figs. 5(a), 6, and 8).

The high-amplitude triangular wave resulted in lower values of coulomb friction, ranging from 34 to 125 J (25 to 92 ft-lb) in the pitch axis and from 12 to 201 J (9 to 148 ft-lb) in the yaw axis. A piecewise linear variation of increasing force (torque) with increasing rotation was observed. This was displayed as a steep slope (K) when motion was reversed, lasting an interval of 0.2°, and a shallow slope (K1) as motion continued. The steep slope K is similar to the slope observed in the low amplitude tests, and it is attributed to the elastic stressing of the interface bond between the rolling and stationary surfaces of the gimbal journal bearing. This type of characteristic is actually that of a simple rotational spring, with sliding after reaching the coulomb friction. The shallow slope K1 is attributed to the linear variation found in the test rig (see Figs. 5(a), 6, and 7).

Environmental conditions were observed to affect the coulomb friction values. Test condition 1 results showed higher values of coulomb friction than test conditions 2 and 3. Furthermore, test condition 2 gave values of coulomb friction greater than test condition 3. From this, it was evident that coulomb friction decreased with decreasing pressure and/or temperature. The decline in coulomb friction leveled off after the pressure and/or temperature were stabilized, at the respective test conditions.

Another phenomenon that was apparent during testing was that, as the frequency increased, the width of the hysteresis loop decreased. This can be seen by comparing the high amplitude curve (frequency of 2.0 Hz) of Fig. 6 with the curves in Fig. 7 (frequency of 1.0 Hz).

It should be noted that the large values of coulomb friction presented in Table II for gimbal 759 yaw axis reflect a suspected deficiency in the quality

of the journal bearing in that particular axis. This was not observed in any other gimbal tested, and was isolated to gimbal 759 yaw axis.

CONCLUDING REMARKS

An investigation was conducted to determine the coulomb friction characteristics of the Centaur launch vehicle gimbal system. Data have been presented for a number of conditions for both pitch and yaw axes. The experimental data showed that torques required to rotate the gimbal had elastic characteristics, where the torques were proportional to the rotational displacement up to a certain value beyond which the gimbal would rotate with small increases in torque. Coulomb friction is defined as the maximum applied torque (breakaway torque) that occurs prior to gimbal sliding. The gimbal friction characteristic is similar to that of rolling friction. Furthermore, environmental effects were shown to have a major influence on the coulomb friction, which decreased with both pressure and temperature. It has also been shown that the elastic characteristics of the gimbal are independent of the input signal.

After a review of the experimental data, it was decided to use the low amplitude and low frequency data for mathematically modeling the gimbal friction characteristics for Centaur autopilot performance studies.

The results of this test are based on the Centaur gimbal system. However, the characteristics may be applied to any launch vehicle gimbal system that incorporates journal bearings.

Further tests will be performed on the Centaur tank structure, where the gimbal is attached, to determine the contribution of tank stiffness to the elasticity of the system.

REFERENCES

[1] RL10 Liquid Rocket Engine, Service Manual, Model RL10-3-3A, Pratt and Whitney Aircraft, Feb. 15, 1982.

[2]Dohl, P.R., "A Solid Friction Model," TOR-0158(3107-18)-1, Aerospace Corporation, May 1968.

[3]Bowden, F.P. and Tabor, D., The Friction and Lubrication of Solids, Part II, Clarendon Press, London, 1964.

[4]Rabinowicz, E., Friction and Wear of Materials, Wiley, 1965.

[5]Bisson, E.E. and Anderson, W.J., "Advanced Bearing Technology," NASA SP-38, 1964.

[6]Antl, R.J., Vincent D.W., and Plews, L.D., "Static and Dynamic Characteristic of Centaur Gimbal System Under Thrust Load," NASA TM X-1205, 1966.

TABLE I. - SUMMARY OF EXPERIMENTAL DATA IN PITCH AXIS

Gimbal number	Waveform	Frequency, Hz	Amplitude,[a] deg	Slope, K		Coulomb friction,[b] CF		Angular velocity,[a] $\dot{\theta}$, deg/sec
				J/deg	ft-lb/deg	J	ft-lb	
Ambient temperature and pressure								
759	Triangle	0.10	0.25	567	418	129	95	0.10
		.50	↓	544	401	118	87	.50
		1.00		529	390	115	85	1.00
		2.00		380	280	113	83	2.00
94	Triangle	0.10	2.00	939	693	125	92	0.80
		.50	↓	580	428	122	90	4.00
		1.00		321	237	117	86	8.00
		2.00		200	148	110	81	16.00
Ambient temperature and vacuum								
759	Triangle	0.10	2.00	603	445	87	64	0.80
		.50	----	----	----	---	--	-----
		1.00	2.00	194	143	75	55	8.00
		2.00	2.00	100	74	73	54	16.00
94	Triangle	0.10	2.00	1128	832	79	58	0.80
		.50	↓	389	287	85	63	4.00
		1.00		274	202	88	65	8.00
		2.00		160	118	85	63	16.00
Cryogenic temperature								
759	Triangle	0.10	0.25	1356	1000	122	90	0.10
		.50	↓	1017	750	115	85	.50
		1.00		881	650	115	85	1.00
		2.00		637	470	115	85	2.00
	Sine	0.10	0.25	1274	940	102	75	0.157
		.50	↓	915	675	↓	↓	.785
		1.00		698	515			1.571
		2.00		407	300			3.142
	Triangle	0.10	2.00	1152	850	34	25	0.80
		.50	↓	373	275	41	30	4.00
		1.00		187	138	47	35	8.00
		2.00		115	85	47	35	16.00
94	Triangle	0.10	0.25	1310	966	113	83	0.10
		.50	↓	1093	806	103	76	.50
		1.00		626	462	98	72	1.00
		2.00		504	372	98	72	2.00
	Sine	0.10	0.25	1474	1087	98	72	0.157
		.50	↓	1201	886	98	72	.785
		1.00		1197	883	98	72	1.571
		2.00		360	265	90	66	3.142
	Triangle	0.10	2.00	1316	971	58	43	0.80
		.50	↓	449	331	60	44	4.00
		1.00		268	198	57	42	8.00
		2.00		157	116	61	45	16.00

[a]Zero to peak.
[b]Peak to peak.

TABLE II. - SUMMARY OF EXPERIMENTAL DATA IN YAW AXIS

Gimbal number	Waveform	Frequency, Hz	Amplitude,[a] deg	Slope, K		Coulomb friction,[b] CF		Angular velocity,[a] $\dot{\delta}$, deg/sec
				J/deg	ft-lb/deg	J	ft-lb	
Ambient temperature and pressure								
759	Triangle	0.10	2.00	1108	817	201	148	0.80
		.50	↓	625	461	183	135	4.00
		1.00		404	298	182	134	8.00
		2.00		237	175	180	133	16.00
94	Triangle	0.10	2.00	834	615	113	83	0.80
		.50	↓	488	360	102	75	4.00
		1.00		309	228	83	61	8.00
		2.00		163	120	72	53	16.00
Ambient temperature and vacuum								
759	Triangle	0.10	2.00	1045	771	184	136	0.80
		.50	↓	675	498	174	128	4.00
		1.00		361	266	172	127	8.00
		2.00		225	166	168	124	16.00
94	Triangle	0.10	2.00	949	700	85	63	0.80
		.50	↓	442	326	79	58	4.00
		1.00		259	191	75	55	8.00
		2.00		144	106	68	50	16.00
Cryogenic temperature and vacuum								
759	Triangle	0.10	0.25	1017	750	203	150	0.10
		.50	↓	1003	740	201	148	.50
		1.00		976	720	202	149	1.00
		2.00		983	725	193	142	2.00
	Sine	0.10	0.25	1028	758	207	153	0.157
		.50	↓	891	657	205	151	.785
		1.00		813	600	201	148	1.571
		2.00		697	514	193	142	3.142
	Triangle	0.10	2.00	975	719	126	93	0.80
		.50	↓	487	359	102	75	4.00
		1.00		324	239	99	73	8.00
		2.00		168	124	98	72	16.00
94	Triangle	0.10	0.25	963	710	77	57	0.10
		.50	↓	831	613	68	50	.50
		1.00		495	365	68	50	1.00
		2.00		373	275	64	47	2.00
	Sine	0.10	0.25	893	659	69	51	0.157
		.50	↓	880	649	68	50	.785
		1.00		675	498	65	48	1.571
		2.00		363	268	61	45	3.142
	Triangle	0.10	2.00	1013	747	15	11	0.80
		.50	↓	335	247	14	10	4.00
		1.00		187	138	14	10	8.00
		2.00		95	70	12	9	16.00

[a]Zero to peak.
[b]Peak to peak.

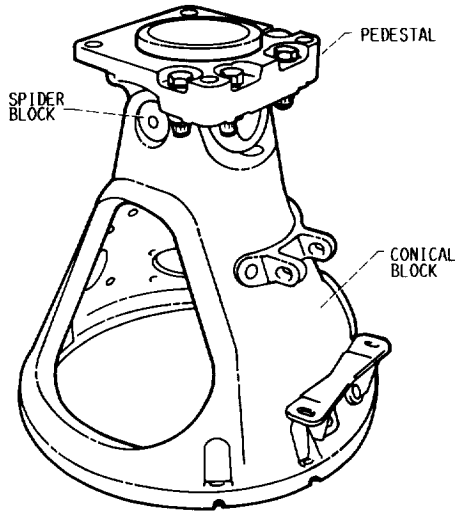

FIG. 1. - ENGINE MOUNT GIMBAL ASSEMBLY.

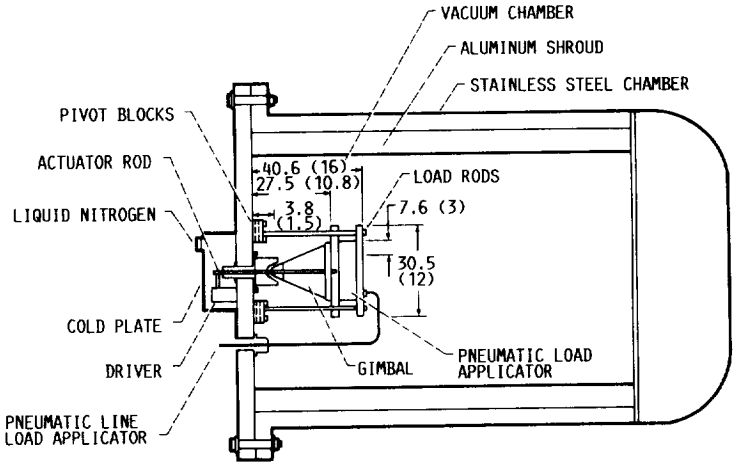

FIG. 2. - GIMBAL FRICTION TEST SETUP. (ALL DIMENSIONS GIVEN IN CM (IN.).)

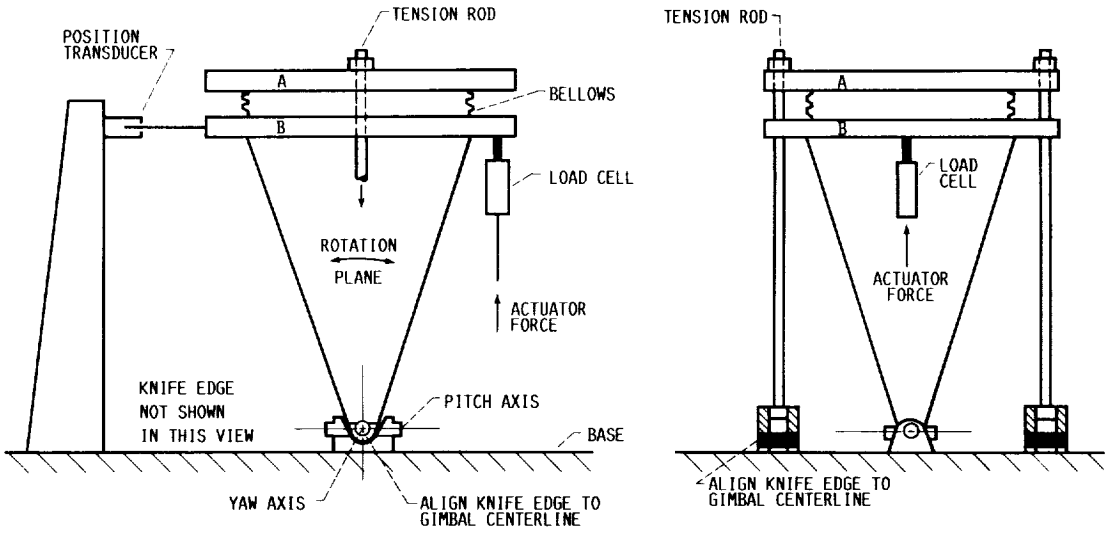

FIG. 3. - GIMBAL FRICTION TEST RIG CONFIGURATION.

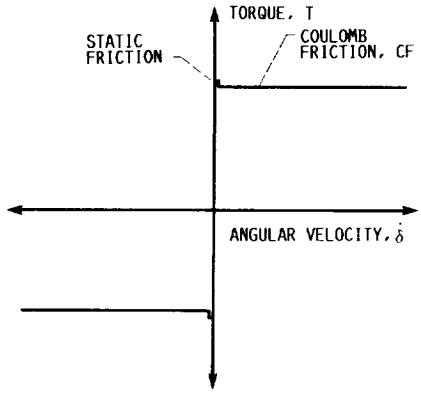

FIG. 4. - CONVENTIONAL DEFINITION OF SOLID FRICTION.

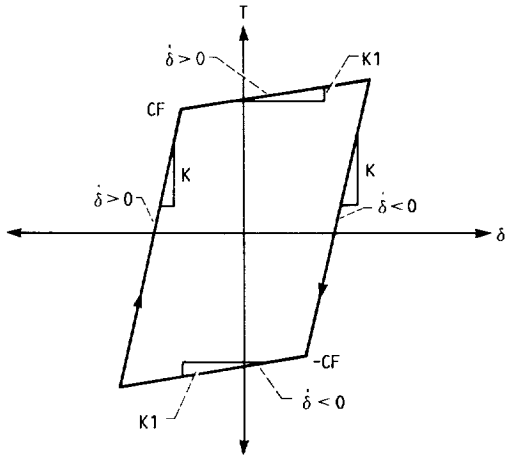

(A) RAW DATA.

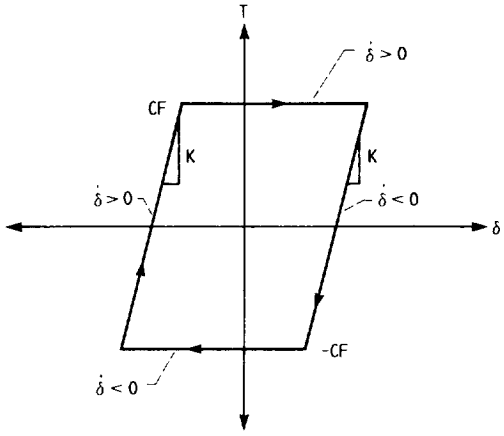

(B) REDUCED DATA.

FIG. 5. - TORQUE AS A FUNCTION OF ROTATION FOR RAW AND REDUCED DATA.

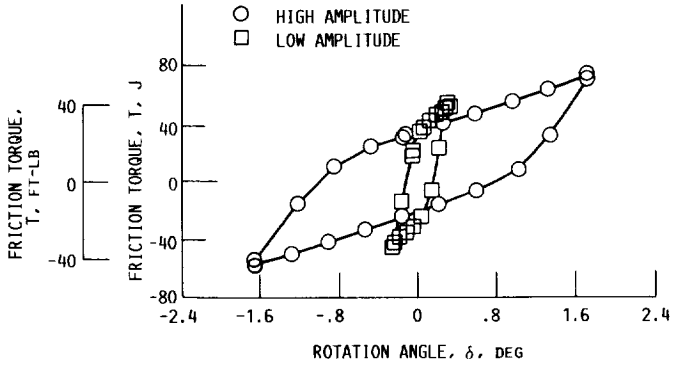

FIG. 6. - TYPICAL GRAPH OF THE CHARACTERISTICS OF EXPERIMENTAL DATA AT HIGH AND LOW AMPLITUDE. FREQUENCY, 2.0 Hz; PITCH AXIS; TRIANGULAR WAVE INPUT.

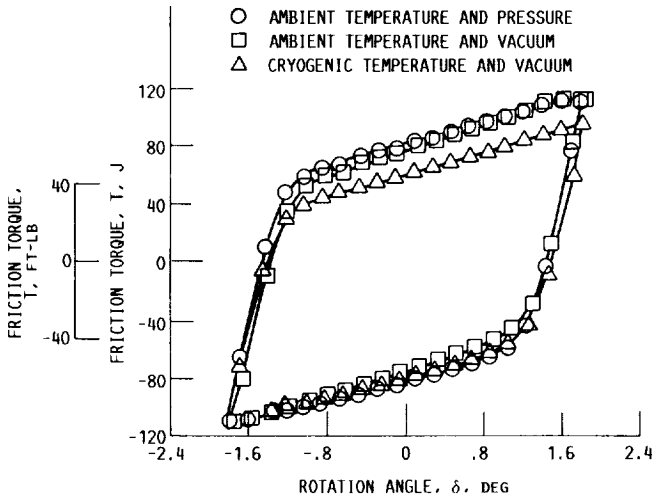

FIG. 7. - GRAPHICAL REPRESENTATION OF THE DIFFERENT TEST CONDITIONS AT ±1.85°. FREQUENCY, 1.0 HZ; PITCH AXIS; TRIANGULAR WAVE INPUT.

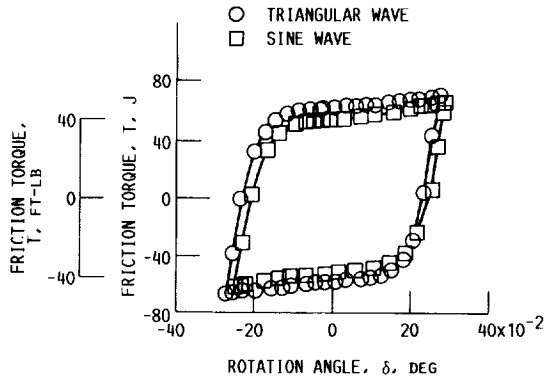

FIG. 8. - GRAPHICAL REPRESENTATION OF THE CHARACTERISTICS OF INPUT SIGNALS, AT 0.25°. FREQUENCY, 0.10 HZ; PITCH AXIS.

1. Report No.	2. Government Accession No.	3. Recipient's Catalog No.
NASA TM-87335		

4. Title and Subtitle	5. Report Date
Centaur Engine Gimbal Friction Characteristics Under Simulated Thrust Load	September 1986
	6. Performing Organization Code: 928-60-02

7. Author(s)	8. Performing Organization Report No.
James W. Askew	E-3080
	10. Work Unit No.

9. Performing Organization Name and Address	11. Contract or Grant No.
National Aeronautics and Space Administration Lewis Research Center Cleveland, Ohio 44135	13. Type of Report and Period Covered: Technical Memorandum

12. Sponsoring Agency Name and Address	14. Sponsoring Agency Code
National Aeronautics and Space Administration Washington, D.C. 20546	

15. Supplementary Notes

16. Abstract

An investigation was performed at NASA Lewis Research Center to determine the friction characteristics of the engine gimbal system of the Centaur upper stage rocket. Because the Centaur requires low-gain autopilots in order to meet all stability requirements for some configurations, control performance (response to transients and limit-cycle amplitudes) depends highly on these friction characteristics. Forces required to rotate the Centaur engine gimbal system were measured under a simulated thrust load of 66 723 N (15 000 lb) and in an altitude/thermal environment. A series of tests was performed at three test conditions: ambient temperature and pressure, ambient temperature and vacuum, and cryogenic temperature and vacuum. Gimbal rotation was controlled, and tests were performed in which rotation amplitude and frequency were varied by using triangular and sinusoidal waveforms. Test data revealed an elastic characteristic of the gimbal, independent of the input signal, which was evident prior to true gimbal sliding. The torque required to initiate gimbal sliding was found to decrease when both pressure and temperature decreased. Results from the low amplitude and low frequency data are currently being used in mathematically modeling the gimbal friction characteristics for Centaur autopilot performance studies.

17. Key Words (Suggested by Author(s))	18. Distribution Statement
Centaur Gimbal Friction	Unclassified - unlimited STAR Category 15

19. Security Classif. (of this report)	20. Security Classif. (of this page)	21. No. of pages	22. Price*
Unclassified	Unclassified		

*For sale by the National Technical Information Service, Springfield, Virginia 22161

National Aeronautics and
Space Administration

Lewis Research Center
Cleveland, Ohio 44135

SECOND CLASS MAIL

ADDRESS CORRECTION REQUESTED

Official Business
Penalty for Private Use $300

Postage and Fees Paid
National Aeronautics and
Space Administration
NASA-451

NASA